Effects of fly ash on mechanical properties of PC girder using reactive andesite aggregates

Tuan Minh Ha, Saiji Fukada, Kazuyuki Torii

Journal of Advanced Concrete Technology, volume 11 (2017), pp. 579-594

Scientific paper

Effects of Fly Ash on Mechanical Properties of PC Girder Using Reactive Andesite Aggregates

Tuan Minh Ha[1*], Saiji Fukada[2] and Kazuyuki Torii[2]

Received 21 July 2017, accepted 27 September 2017 doi:10.3151/jact.15.579

Abstract

In the Hokuriku region, alkali-silica reaction (ASR) caused severe degradations in many concrete bridges. However, criteria for repair and replacement works of these structures are still unclear. For the development of damage evaluation procedure, it is necessary to investigate the load-carrying capacity of prestressed concrete (PC) girders affected by ASR-induced deterioration in actuality. This study constructed two full-size PC specimens from the high-early-strength Portland cement and reactive aggregates, and then exposed them to outdoor environmental conditions. One of them was specially mixed with a controlled amount of fly ash. After one and a half years of outdoor exposure, destructive loading tests were carried out to investigate the difference in loading capacity of the girders. From results of the long-term exposure and the tests, the flexural strength and the rigidity of the specimen with fly ash were not degraded while ASR was also effectively suppressed. In addition, cylindrical concrete cores were taken at different positions of both girders to analyze the relationship between mechanical properties of concrete such as compressive strength, static elastic modulus, and ultrasonic wave propagation speed. Results of the coring test showed that the mechanical properties of concrete cores varied according to their collecting positions and directions.

1. Introduction

During the previous years, the degradation due to alkali-silica reaction (ASR) in concrete structures has become a global concern. Many structures such as bridges, dams and concrete barriers were affected. Stanton (1940) showed the loss in engineering features due to ASR for the first time in the U.S. in 1940. Since then, an increasing number of regions with different climates where civil engineering works experience deterioration problems as a result of the ASR has been reported from Argentina, Switzerland, Netherlands, Korea, Japan, Thailand and other countries (Marfil and Maiza 2001; Leemann *et al*. 2005; Hong *et al*. 2007; Gasparotto *et al*. 2011; Hirono *et al*. 2016). In Japan, mineralogical and geological studies show that many reactive aggregates in the soil are widely distributed throughout the country (Yamada *et al*. 2011). Particularly in the Noto region, there is a wide distribution of andesite, which is the primary cause of ASR degradation in bridges (Torii *et al*. 2007, 2010, 2012). Since 1982, ASR has been observed in highway structures in this region, where deicing salts (mainly NaCl) are used in the winter (Katayama *et al*. 2004). The added alkali contents from deicing salt and seawater have raised concrete alkali levels above acceptable limits, excepting concrete in cooperation with mineral admixtures such as blast-furnace slag or fly ash. Up to recent years, not only the Noto region but many infrastructures in the Hokuriku region (Fukui, Ishikawa, Toyama, and Niigata prefectures) were also degraded by ASR (Torii *et al*. 2016a; Kubo *et al*. 2016). The reaction starts the expansion of reactive aggregate by forming a swelling gel of alkali silicate hydrate (N(K)-C-S-H). The ASR gel increases in volume, exerting significant pressure within the material, which causes spalling, cracking, and loss of strength in the concrete and rebar. The relations between the characteristics of ASR-induced damage and the reduction of the elastic modulus have been proved by many previous studies (Giaccio *et al*. 2008). Detailed information on the cracking behaviors of many concrete structures damaged by ASR was presented in studies of Ono (1988) and Tordoff (1990). Cracking in concrete due to ASR takes various patterns. In the portions of a reinforced concrete (RC) structure with little or no surface reinforcement, cracking tended to be irregular and maplike. The authors also suggested that, while notable and extensive corrosion had not yet been recognized, appropriate repair techniques should be considered to protect the damaged structures from further deterioration. Therefore, the development of maintenance management methods became an important topic in the literature in recent years.

Regarding modeling approaches, the ASR gel production, expansive behavior of ASR, and its damage have been studied recently (Gong *et al*. 2017; Takahashi *et al*. 2016; Saouma 2014). Saouma (2014) proposed finite element method (FEM) models for ASR, considering the micro-chemical reactions while attempting to apply models to structural levels. Two years later, by utilizing a computation scheme of multi-scale

[1]PhD Candidate, Graduate School of Natural Science and Technology, Kanazawa University, Japan.
*Corresponding author:
E-mail: minhtuan09xdbk@gmail.com
[2]Professor, School of Environmental Design, Kanazawa University, Japan.

poro-mechanics, Takahashi *et al*. (2016) carried out sensitivity analyses with the permeation of produced silica gel. Since structural concrete usually experiences combined effects of ASR, carbonation, freeze-thaw cycles, steel corrosion, and high cycle fatigue loads (Gong *et al*. 2017), the concrete degradation is complex. Indeed, ASR and steel corrosion will consume water on which frost damage also relies. In 2017, Gong *et al*. successfully modeled the interaction between freeze-thaw cycles and ASR form the micro-structural level, taking the ice formation and ASR gel intrusion in pores into account, as well as the effect of entrained air.

For the experimental and monitoring approaches, the effects of blast furnace slag on the loading capacity of prestressed concrete (PC) specimens using reactive aggregates have been confirmed by Kunitomi *et al*. in 2015. Besides, it is now generally accepted that an appropriate use of fly ash can prevent expansion due to ASR in concrete (Torii *et al*. 2016b). An increase in a level of replacement of a particular fly ash further reduced the expansion of concrete compared with the concrete without fly ash (Shehata and Thomas 2000). Since the Hokuriku region is currently able to provide a high quality fly ash stably (Hashimoto *et al*. 2013, 2015), the efficient use of fly ash helps improve the concrete durability and reduces the environmental burden as well as promote the regional industry due to the benefits of self-sufficiency. For example, together with the large-scale renewal project of Hokuriku Expressway using fly ash concrete precast PC slabs, the construction of new PC girder bridges in the local region also utilized fly ash for mitigating deterioration caused by ASR (Yamamura *et al*. 2016). Indeed, the countermeasures for newly built bridges against ASR have achieved success. However, the evaluation criteria for repair and recovery work have not been clarified as regards to ASR-affected structures. Therefore, to obtain these materials, it is necessary to study the loading capacity and mechanical properties of full-size PC girders degraded by ASR. Over the years, many researchers have taken the loading tests on both ASR-degraded PC and RC specimens.

Regarding RC structures, Swamy and Al-Asali (1989) carried out destructive load tests on RC beams, which were made with reactive coarse and fine aggregates, to determine their structural behaviors (load versus deflection) under significant ASR expansions. Their outcomes showed that the initial stiffness and ultimate load-carrying capacity were not obviously influenced by ASR and loading conditions, whereas ASR-induced reductions in the tensile strength and dynamic modulus of elasticity of concrete beams could be perceived. Later, Shenfu and Hanson (1998) made six 1500 mm long reinforced concrete beams and immersed them in a cyclically-heated alkali solution in one year to accelerate ASR. Particularly, three of them were produced with the reactive concrete, while the nonreactive concrete was utilized for the other beams. Although ASR-caused cracks occurred on specimens made with the reactive aggregate after six months of the immersion, they performed nearly the same flexural strengths as the nonreactive beams did. Moreover, the influence of ASR on the flexural loading capacity of preloaded and cracked beams was also perceived to be insignificant. The fracture mechanism of reinforcing steels in the case of concrete structures damaged by ASR was studied thoroughly by Miyagawa *et al*. (2006). The authors introduced the results of the investigation on the fracture mechanism, nondestructive testing methods, and repair and strengthening methods for damaged concrete structures. Particularly, the steel bar rib shape and the bending radius were considered to have a significant causal influence on steel bar fractures due to ASR. Moreover, weather conditions (such as rainwater, sunlight, and ambient temperature) caused obvious effects on ASR-induced deterioration which also tends to be particularly severe at locations where the number of steel bars is relatively small. As long as ASR-caused expansion does not break reinforcing steels, the soundness of a structure is considered not to be endangered. In 2012, Wang and Morikawa studied the deterioration situation of concrete members due to ASR and its influence on shear failure mechanism and shear resisting performance of 1200 mm RC beams in both experimental and numerical approaches. The experimental results showed that undesirable shear collapse modes were obtained and the bond slip was easy to occur in RC beam with ASR-induced cracks along the tensile reinforcing bars. Besides, ASR deterioration was considered as the thermal strain model, which utilized a series of temperature values and the linear thermal expansion coefficient of the concrete element as inputs for simulating the expansion caused by ASR degradation. Their analysis results showed a good agreement with the experimental data regarding the load-displacement response, crack pattern and rebar strain distribution. As another study of Hajighasemali *et al*. (2014), the influence of ASR on overall serviceability, strength, ductility and deformability on RC beams under service load conditions was investigated by considering creep and ductility phenomena. Twelve 1100 mm long RC beam specimens were initially produced utilizing to nonidentical concrete mixtures containing reactive aggregates (R) and nonreactive aggregates (N). The specimens were later subjected to flexural testing after 360 days of accelerated ASR conditioning. For ductility and deformability analyses on the basis of comparison of R and N beams, ductile indices related to displacement, curvature, and energy were estimated by considering load-deflection and moment-curvature curves. Their conclusions proved that ASR has a significant effect on the R beams (where cracks occurred at lower loads) and, the N beams were stronger than their equivalent R specimens at final loading.

The structural performance of the prestressed beams made of concrete affected by ASR-affected by ASR was described by Kobayashi *et al*. (1988) in comparison with

those of corresponding healthy beams. Ten 1600 mm PC beams made of two types of concrete with alkali-silica reactivity and sound concrete under an accelerated curing condition of 40 ºC and 100% RH were subjected to long-term monitoring of changes in steel strains and destructive tests with shear span to effective depth ratio of 2.5 and 4.0. As their findings, longitudinal ASR expansion could be restrained by the introduction of prestressing force, although the effect depends strongly upon the amount of the prestress. Also, the reduction in the ultimate strength of ASR beam was approximately 10% compared with that of the sound beam, even when the tensile strain in vertical stirrup exceeded 1000×10^{-6} and many longitudinal cracks occurred. Takebe et at. (2013) verified the effects of the presence or absence of ASR deterioration on shear strength of concrete members using two different PC specimens (height 300 mm × width 300 mm × length 2000 mm). The controlled beam contains normal aggregate and the other has ASR reactive aggregate in its mixture. Before destructive loading tests, both specimens were exposed outdoors for further progress of ASR deterioration in approximately 3 years. Their findings showed that both specimens failed in flexural mode, with final load of ASR-affected beam being about 7 % lower than that of the normal one. As recent efforts, Hiroi *et al*. (2016) carried out the flexural loading test on real-scale large PC beams (height 1250 mm × width 1200 mm × length 7000 mm) which were exposed to 7.5 years of deterioration. After the tests, concrete core samples were collected from the beams to evaluate mechanical properties of ASR-affected concrete. Their outcomes show that the mechanical values decreased even in the longitudinal direction where there was confinement due to the prestress. Moreover, the decreases in Young's modulus and tensile strength were more obvious than that of compressive strength, and the decrease rate was higher in the vertical cores in which confinement was absent, as compared to the longitudinal cores. As another attempt of the same study, Yokoyama *et al*. (2016) performed a visual observation of internal cracks in the cut section. Although many ASR cracks could be easily observed in the surface areas of the beam, most of them occurred outside the stirrups, with almost no further progress into the inside. Besides, the development of flexural cracks was partly interrupted by the appearance of ASR-induced horizontal cracks in the cover concrete, that resulted in a relatively decrease in stiffness.

In addition, for the investigation and inspection of an actual bridge in which main girders were placed side by side as shown in **Fig. 1**, concrete cores are usually taken from side surfaces which might not provide enough information about the load-carrying capacity and stiffness of the girder accurately. As the development of cracks in PC girders is also governed by the restraints of the PC strands, the mechanical properties of concrete might differ from prestressing direction (girder-axis direction) to transverse direction (Kunitomi *et al*. 2015). Therefore, it is necessary to study this anisotropy of concrete in degraded PC girders.

After all, none of above studies have been taken on the real-scale PC specimens using reactive aggregates to find the difference in flexural capacity due to the fly ash content. This study aims to investigate how the structural properties and load bearing capacity of PC girders, which were affected by varying degrees of ASR-induced damages, change with and without fly ash. Two full-scale PC girders were conducted by the mixture of reactive aggregates and high strength Portland cement for the present study. Particularly, one of them was mixed with an additional amount of fly ash. After one and a half years of the exposure, destructive bending tests were carried out so as to clarify the difference in flexural capacity. In addition, after the bending tests, a large number of concrete cores were taken from both girders to estimate the relationship between mechanical properties of concrete such as compressive strength, static elastic modulus, and ultrasonic wave propagation velocity. Based on the obtained results, this study clarified mechanical properties of PC girder with and without fly ash affected by ASR deteriorations.

2. Description of the PC girders

2.1 Shape and exposure conditions

The PC girders produced in this study are the full-size JIS A5373-AS09 girder. Both girders have same side and cross-sectional views as depicted in **Fig. 2**. From this figure, the girders have a length of 9600mm, a cross-section with an upper-edge width of 640 mm, a lower edge width of 700 mm, and a height of 450 mm. It should be noted that the sheath holes for lateral tighten-

Fig. 1 Cracks occurs along with the PC strands (bottom surfaces).

Table 1 Material properties of two girders.

Material	Symbol	Specification
Cement	C	Early-strength Portland cement, density: 3.14 kg/cm^3, specific surface area: 4510 cm^2/g
Admixture	FA	Classified fly ash (Nanao Ohta Thermal Power Station), density: 2.43 g/cm^3, specific surface area: 4500 cm^2/g, ignition loss value: 2.0 %
Fine aggregate	S	River sand (from the Joganji River), density in saturated surface-dry condition: 2.61 g/cm^3
Coarse aggregate	G	Crushed stone (from the Joganji River), density in saturated surface-dry condition: 2.61 g/cm^3
High-performance water-reducing agent	SP	Mighty 21LV (Kao Chemicals)
AE agent	AE	Vinsol (Yamaso Chemicals)

Table 2 Mixture properties.

Name	Water-binder ratio W/B (%)	Fine aggregate percentage s/a (%)	Unit (Kg/m^3)						SP (B*%)	AE (B*%)
			Water W	Binder B		Sand S	Gravel G	NaCl		
				Cement C	Fly ash FA					
H girder	38.7	46.3	150	388	-	822	955	25.5	1.00	0.006
FA girder	34.8	44.6	150	366	65	770	955	25.5	1.20	0.02

ing of transverse beams are not provided. Regarding PC strands, each objective girder contains sixteen strands (SWPR7BL1S 12.7 mm) arranged longitudinally in three layers. Specifically, four strands were put as the first layer in the compression area while the other two layers consisted six strands in each were arranged in the tension area. Both objective girders were conducted by the pre-tensioning method. In this study, high strength Portland cement was utilized for both girders. One of them was particularly mixed with an addition amount of fly ash (FA girder), while the other girder without fly ash was named as H girder. Both H and the FA specimens have the same profiles and dimensions of strands and stirrups. After 14 hours of steam curing at 50 ℃, the tendons were released from external frames then the PC girders were continuously moistened indoor for about one week. Following the initial curing, they were placed in the sunshiny area of Kakuma campus in Kanazawa city so as to be exposed to outdoor environment for one and a half years, as shown in **Fig. 3**. During the exposure period, the average ambient temperature of Kanazawa city varied from approximately ~13.3 °C in April to ~27 °C in August 2015 (during summer) and then decreased gradually by ~22 °C from the high temperature to ~5 °C in January 2016 (between summer and winter), before rising gradually again to ~27.5 °C in August 2016 (summer season). The average ambient humidity was around 70% (Japan Meteorological Agency 2016).

2.2 Materials

Materials used for the PC girders are summarized in **Table 1**. River sand and crushed stones from the Joganji River were used as reactive aggregates, which contain mainly cristobalite and opal. In addition, fly ash with an average grain size of up to 7μm was taken from Nanao Ohta Thermal Power Station of Hokuriku Electric Power Company.

2.2.1 Mixtures

Both specimens were cast with mixtures shown in **Table 2**. H girder utilized only early strength Portland cement. Regarding FA girder, the replacement rate of fly ash to binder was set to 15% based on the consideration of quality and workability of classified ash from the previous research results (Yamamura *et al*. 2016), which also confirmed the effectiveness of fly ash to mitigate ASR. Moreover, to promote the expansion of concrete by ASR, 25.5 kg/m^3 NaCl in an equivalent amount of 13 kg/m^3 Na_2O was added to the mixture of each girder.

2.2.2 Material characteristics of concrete

Both girders had the same design compressive strength which were 35 N/mm^2 and 50 N/mm^2 at the ages of 1 day and 14 days after casting, respectively. **Table 3** shows the compressive strength of H girder and FA girder at the time of stress transferring, seven days and 28 days of age. As shown in this table, H girder had higher compressive strength than FA girder at 28-day age.

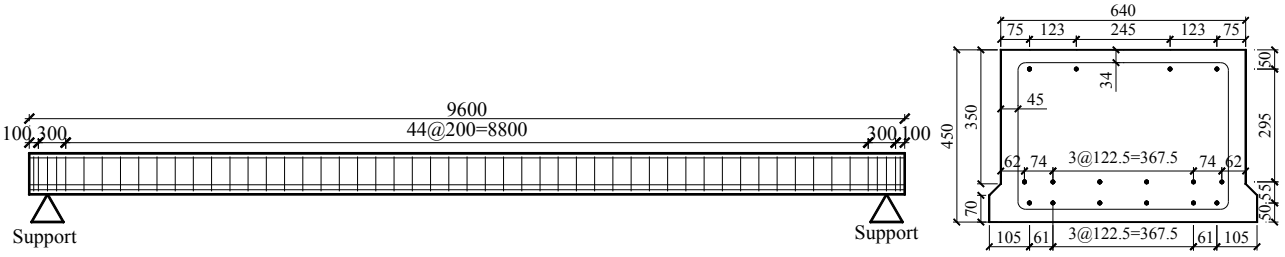

Fig. 2 Diagram of PC girders (unit: mm).

2.2.3 Material characteristics of steels

Material characteristics of steels are shown in **Table 4**. SD295 D10 rebars were used for stirrups at 200 mm intervals while sixteen high strength steel wires SWPR7BL(1S 12.7 mm) were employed as strands used for prestressing. After 14 hours of casting, the strands were released from external frames and their tensile stresses of 1271 N/mm^2 were transferred to the concrete.

3. Deterioration situations of PC girders before the loading test

3.1 Development of ASR-caused cracks

Crack patterns of H and FA girder before the loading test (after one year and a half years under outdoor exposure) are shown in **Fig. 4(a)-(b)**. Black lines illustrate crack width range of 0.3–0.8 mm while crack widths over 0.8 mm are shown as red lines. On the side surfaces of H girder, cracks occurred not only along the longitudinal direction but also along with the three layers of the tendons. On the top surface, longitudinal cracks also appeared along with the upper-tendon layer. However, a few cracks could be observed on the lower surface. The acceleration of ASR-induced cracks on the top and side surfaces as described above was considered to be due to the influence of water and insolation. Moreover, alligator cracks were mainly observed at the girder end, where no prestress was introduced because of the influence of the adhesion transmission length of tendons, which was considered as 65 times the strand diameter (φ = 12.7 mm). Regarding FA girder, cracks appeared partially near the ends and on the side surfaces. Because the number of cracks was considerably small, the expansion of ASR was effectively suppressed due to fly ash content.

Fig. 3 Exposure condition of the PC girders at Kakuma campus.

Table 3 Compression strength of concrete (unit: N/mm^2).

	Stress transferring	σ 7	σ 28
H girder	59.3	70.3	79.8
FA girder	54.4	65.9	77.4

Table 4 Material characteristics of steels (unit: N/mm^2).

	Yield stress	Tensile strength
SD295 D10	375	512
SWPR7BL1S 12.7 mm	1832	2015

3.2 Upward vertical displacement

Figure 5 shows changes in convex curvature (upward

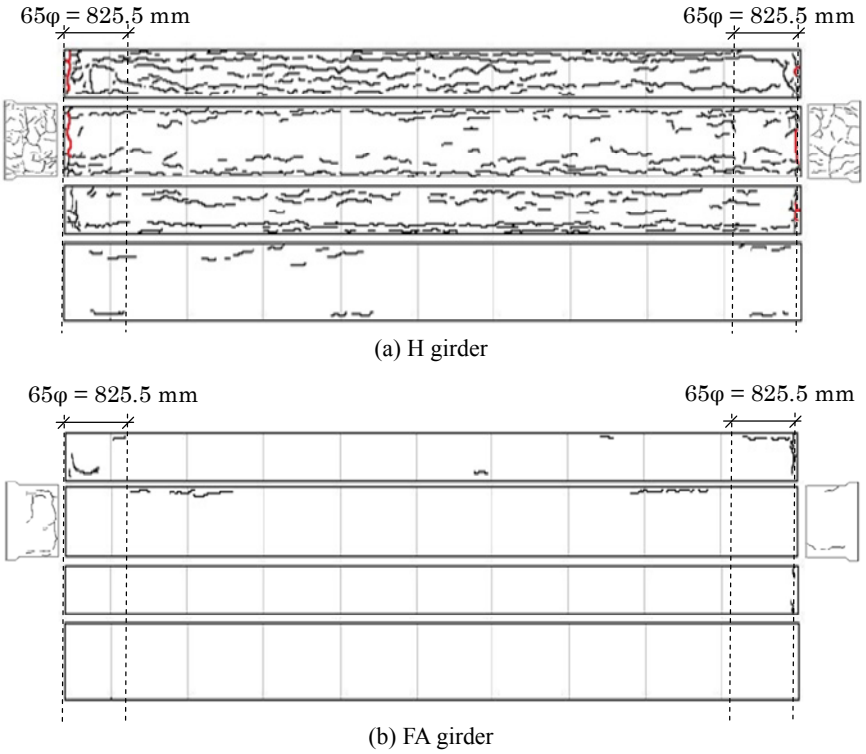

(a) H girder

(b) FA girder

Fig. 4(a)-(b) Crack patterns of both girders (From top to down: north side surface, top surface and both surfaces near both ends, south side surface and bottom surface) and the adhesion transmission length of tendons (approximately 825.5 mm) (unit: mm).

vertical deflection) in the middle of the span of H and FA specimens during the exposure period, which was measured by stretching a leveling string (**Fig.6**) between both ends. As regards H girder, the convex displacement increased up to approximately 13 mm before starting the load test. Meanwhile, almost no variation of the convex curvature over time was observed in FA specimen mixed with fly ash. This monitoring result was also confirmed by previous researchers (Onozato *et al*. 2006; Kunitomi *et al*. 2015). Based on monitoring development of cracks in H girder, this study considered that ASR was accelerated by the penetration of water and the insolation. Because the top surface and both side surfaces were directly exposed to the sun, they suffered higher influences of solar radiation and rain than the bottom surface. Consequently, there were differences in ASR-induced expansion ratio of concrete between surfaces. Changes in the expansion ratio during the follow-up period of both girders are discussed in the flowing section. In addition, regarding the detail of PC strands, four strands were put as the first layer in the compression area while the other two layers consisted six strands in each were arranged in the tension area, as indicated in **Fig. 2**. Therefore, the upward curvature was generated not only by the difference in expansion amount but also by the difference in the tensioning forces of the PC strands between the upper and the lower concrete parts.

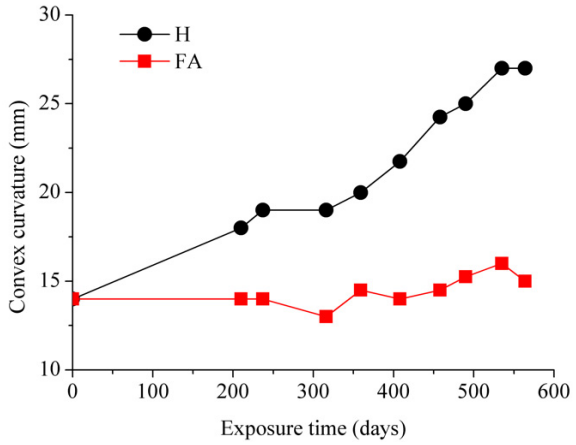

Fig. 5 Changes in the convex curvature.

3.3 Expansion rates

In this study, the progress of ASR deterioration in the PC girders was also observed by monitoring expansion ratio of concrete. Specifically, the ratios in the longitudinal direction (girder-axis direction) and the perpendicular direction of all concrete surfaces (upper, side and bottom surfaces) were measured near the supports and the span center as shown in **Fig. 7**. For each girder, 78 gauge plugs were affixed to the measurement positions then the measurement was performed periodically using a digital type contact micron strain gauge (**Fig. 8**). For tracking the variation of concrete expansion due to ASR, twelve tests were performed from July 2015 to October 2016, and there were 2880 valid sets of measurement data. The ratio was calculated by a change in the distance between two plugs (initial length = 100 mm). **Figures 9** and **10** show the variation in measurement results of both girders in the longitudinal and perpendicular directions over time, respectively. Each value indicated in these figures is the average of all results obtained from strain gauges mounted on the target surface in each measurement. From these figures, the expansion ratio of H girder increased in the order of the bottom surface < the side surfaces < the top surface. Regarding FA girder, this value reduced greatly at all parts. Moreover, when comparing the measured data on the top surface of H girder, the expansion ratio in the transverse direction was

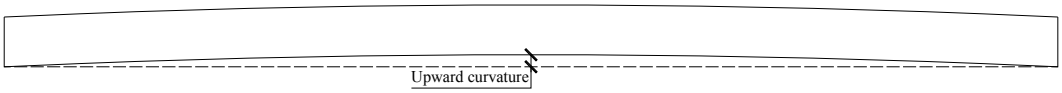

Fig. 6 Measurement of Convex curvature.

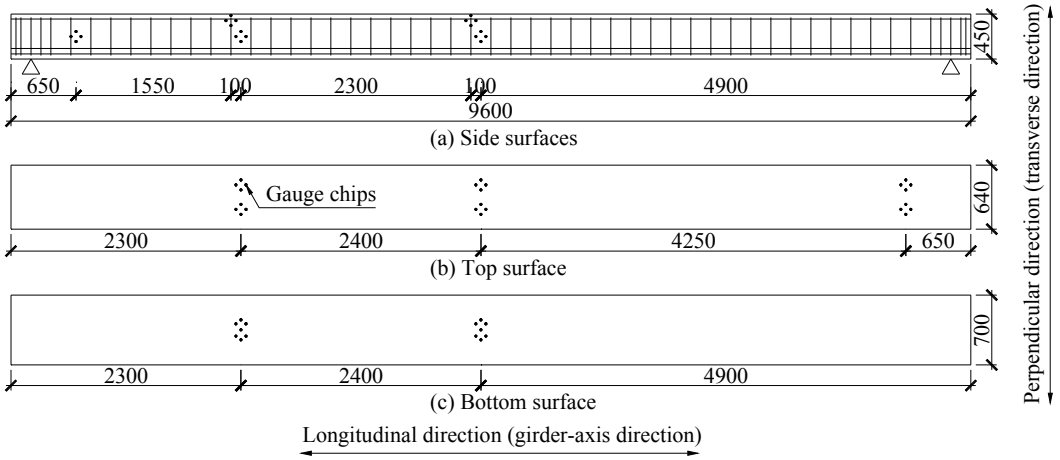

Fig. 7(a)-(c) Measurement locations (unit: mm).

measured as 0.35% or more before the loading test, whereas it was 0.04% or less in the longitudinal direction. Therefore, because the expansion ratio in the transverse direction of H girder was higher than in the longitudinal direction, there was a relation between the expansion ratio of concrete and the formation of longitudinal cracks owing to ASR.

4. Loading test

4.1 Testing method

Regarding the test setup, as shown in **Fig. 11**, each specimen with a span length of 9200 mm was subjected to the four-point bending test in which loads were applied at two points in the middle of the span. The testing girder was simply supported by two round steel bars. In addition, measurement items were load, deflection (vertical direction), crack development (girder axis direction) and concrete surface strain. The arrangement of measurement points is also summarized in this figure.

4.2 Load – displacement relationship

Figure 12 shows the relationship between applied load and vertical displacement at the span center of H and FA specimens. As references, the design values of crack initiation load (126kN) and the bending fracture load (291kN) are also indicated in this figure. As a result of an examination of structural behavior in the elastic range, there was a difference of about 10% in the flexural rigidity between two girders. Specifically, the flexural rigidity of H and FA specimens were calculated as 11.5 kN/mm and 12.8 kN/mm when the applied load reached 50 kN, respectively. As the results of the loading tests, the final load of H and FA girders were recorded as ~312 kN and ~330 kN, respectively, which causing failure in the upper extreme fiber of concrete as showed in **Figs. 13(a)-(b)**. Therefore, the load-carrying capacity of H girder was smaller by about 5% than of FA girder.

(a) Contact micron strain gauge

(b) Gauge chip setup

Fig. 8 Expansion rate measurement.

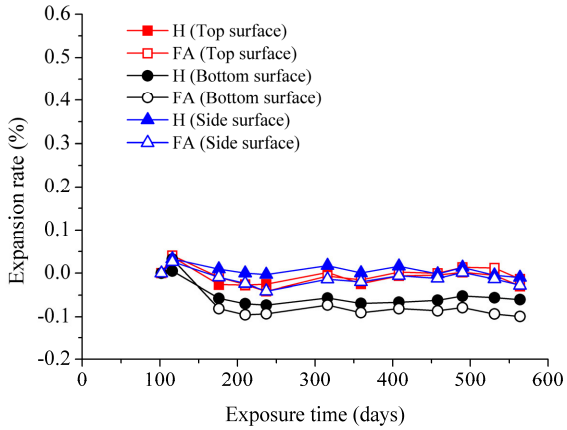

Fig. 9 Variation of expansion rate in longitudinal direction.

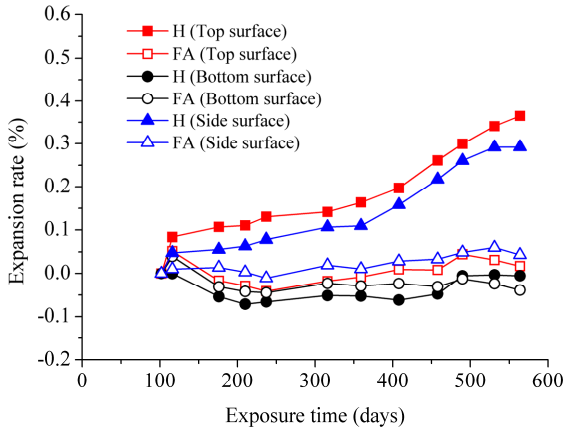

Fig. 10 Variation of expansion rate in transverse direction.

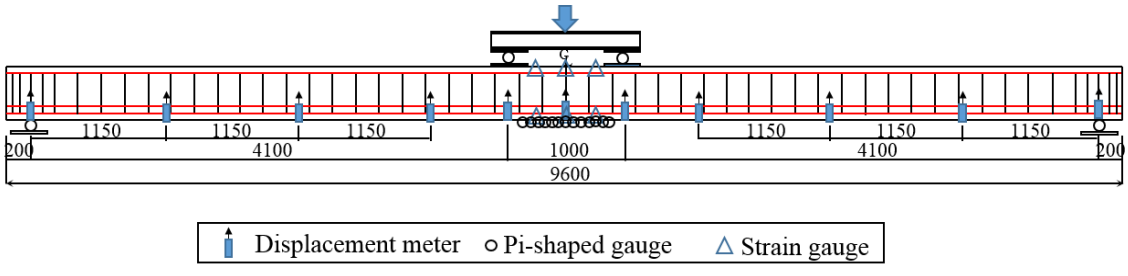

Fig. 11 Overview of loading test setup (unit: mm).

Compared to the specimen mixed with fly ash, the toughness of H girder was deteriorated by the influence of ASR. This 5% reduction in the loading capacity is consistent with results of previous studies conducted in actual bridges (Tomiyama *et al*. 2011; Takebe *et al*. 2013). However, a prior research of Onozato *et al*. (2006) proved that the flexural strength did not decrease because the expansion of ASR was restrained by prestressing force. This outcome was not confirmed in the present study.

The load-strain relationships of concrete on the top and bottom surfaces at the span center are presented in **Fig. 14**. From results of the experiment, the crack initiation load of H specimen was lower than of FA specimen (170kN compared to 190kN, respectively). Although a slight difference in structural behavior between two girders was observed in the elastic range, after the generation of initial crack, the strain of concrete on the upper edge (compression zone) of H girder increased in higher rate in comparison to FA girder. Furthermore, the neutral axis depth from the top edge in the elastic range was calculated to be 227.5 mm for H specimen and 228.7 mm for FA specimen, which was close to the effective area depth of concrete estimated as 228.2 mm. Therefore, ASR-induced cracks on the top and the side surfaces of H girder did not affect the moment of inertia in the elastic region.

Furthermore, in a comparison to the design, it is revealed that both specimen performed higher values in both crack initiation load and bending fracture load. Therefore, even if many cracks owing to ASR appeared on the girders, the steel cables were not broken and corroded after the exposure period. In addition, the bonding separation between steel and concrete did not occur. Although the load-carrying capacity was not significantly deteriorated, it is necessary to establish a maintenance management for these specimens to avoid further damage.

4.3 Crack observation test after the loading test

Figures 15(a)-(b) show crack patterns after the loading test of H and FA girders. Regarding figures of side surfaces, a selected mesh size was 100 mm for vertical direction (50 mm mesh was used for only the top fiber) and was 200 mm for girder-axis direction. As shown in **Fig. 15**, red lines express cracks owing to the load test, and black lines express stripping parts at midspan. The maximum crack interval in pure bending areas of H and FA specimens was approximately 230 mm. Another attractive result was the development of flexural cracks during the test. Since there were many longitudinal cracks caused by ASR on the top and side surfaces of H specimen, vertical cracks owing to applied loads did not continuously propagate upward (**Fig. 16**). Therefore, it was thought that longitudinal cracks interrupted the development of bending cracks. However, an investigation of cut cross sections, which is described in the next section, shown that due to the shallow depth,

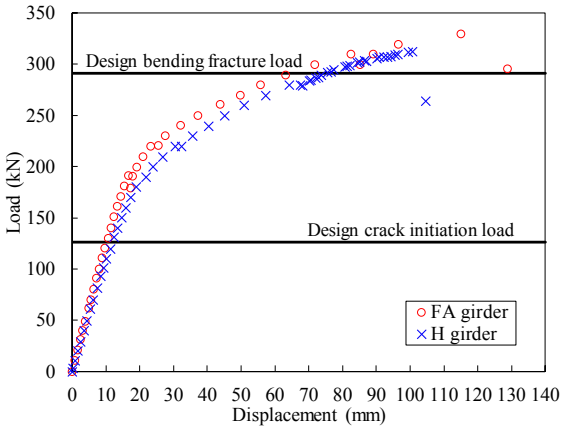

Fig. 12 Load-displacement relationship at midspan.

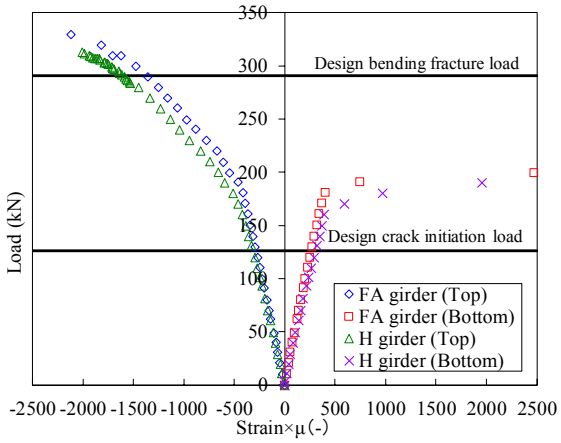

Fig. 14 Load-strain relationship.

(a) FA girder (b) H girder

Fig. 13 Compressive failure mode at the span center of girders at the final loads.

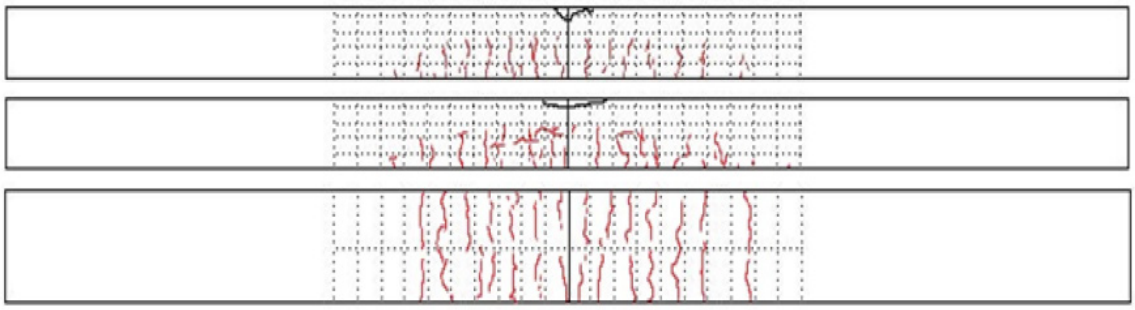

(a) H girder

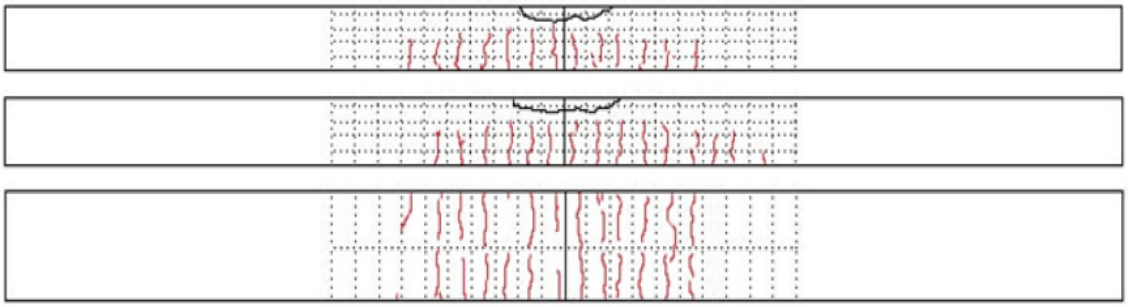

(b) FA girder

Fig. 15(a)-(b) Crack pattern due to loading test (from top to down: north-side, south-side and bottom surfaces).

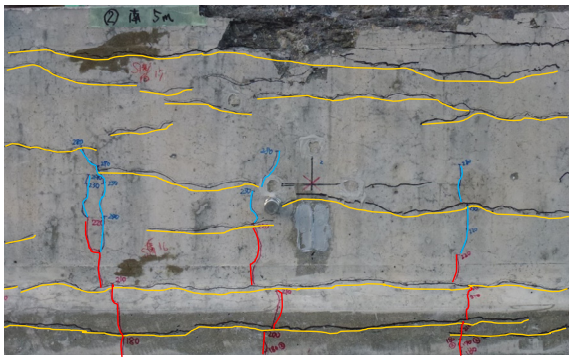

Fig. 16 Crack pattern at the span center after loading test.

longitudinal cracks could not hinder the progress of bending cracks.

4.4 Investigation of the cross-section

To evaluate the condition of inner surfaces after the load test, each girder was cut into three pieces with lengths of 3150 mm, 3300 mm and 3150 mm by a wire saw. **Figure 17** shows a cut surface of H girder between its support and the span center. In this figure, yellow lines show ASR-induced cracks, and green lines show transverse cracks observed on the upper side of tendons in the compression area. Red dots indicate PC strands. From observation results, the depth of ASR-induced cracks along the girder-axis direction varied from 5 to 20 mm on the side surfaces and the top surface, whereas no crack was found out in the area surrounded by stirrups. Moreover, no breaking of tendons was confirmed, whereas transverse cracks were significantly observed on the upper side of tendons in the compression area. After the bending test, for ascertaining the corrosion condition of PC strands, peeled concrete areas of both samples were taken away. However, no steel corrosion could be observed.

5. Diagnosis ASR-induced deteriorations using drilled cores

5.1 Overview of experiment setup

After the girder had been cut into three pieces, cylindrical core samples were collected from both girders at

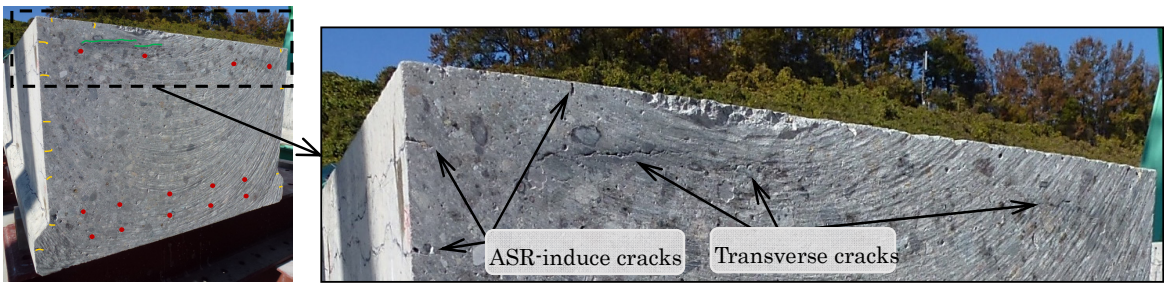

Fig. 17 A cut cross-sectional view of H girder.

positions near support (end part) and at positions around the inner area between two pieces (central part) so as to investigate the mechanical properties of concrete. At each area, six cores along the girder-axis direction (longitudinal direction) and six cores along the direction perpendicular to the girder-axis direction (transverse direction) were collected for the compression tests. In addition, four more samples were collected at central area in both investigate directions for the expansion tests. Each concrete core with a diameter of 55 mm and a length of 110 mm was taken from the surface of concrete about 30 mm. **Figures 18(a)-(c)** show the sampling position. The relation between the reactivity of aggregate and ASR deterioration degree was examined by the immersion method in 1N · NaOH solution (ASTM C1260; Oberholster and Davies 1986; Fournier and Bérubé 1991a, 1991b). Furthermore, the generation of ASR gel, which becomes yellow-green under ultraviolet (UV) light, was observed by the fluorescent visualization method (Sannoh *et al*. 2013). As another observation, thin slices (thickness 20μm) of concrete were taken from the cores and helped investigate the reactive condition of aggregates and the generation of fine cracks on the surface and inside of the cores.

5.2 Cracks and the reactivity of aggregate

Figures 19(a)-(d) indicate observation results of concrete cores of both girders obtained by the fluorescent method. The tested cores were the upper cores taken longitudinally in the central parts of the girders. As the results, regarding the specimen of H girder, the ASR gel under UV light appeared as yellow-green around andesite particles. However, no fluorescence was observed on samples taken from FA girder. In addition, **Fig. 20** shows observation results by a polarized microscope. Regarding H specimen, andesite particles from sand and gravel of the Joganji River reacted strongly, and many fine cracks (about 0.02 mm in width) occurred from broken pieces of aggregates to cement paste. Conversely, andesite particles reacted slightly while no trace of ASR was observed with respect to FA girder. In both girders, no formation of ASR gel was found in the surface layer (about 20 mm) of both specimens. It was inferred that ASR was suppressed in

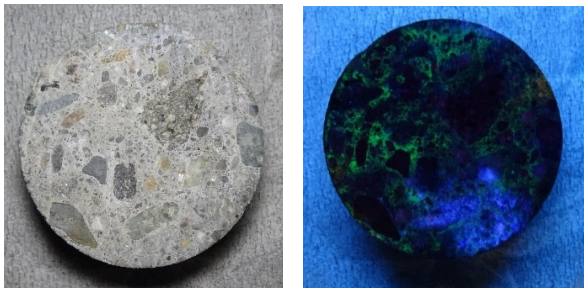

(a) white light (H girder) (b) UV light (H girder)

(c) white light (FA girder) (d) UV light (FA girder)

Fig. 19 Observation results of concrete cores by gel fluorescence method.

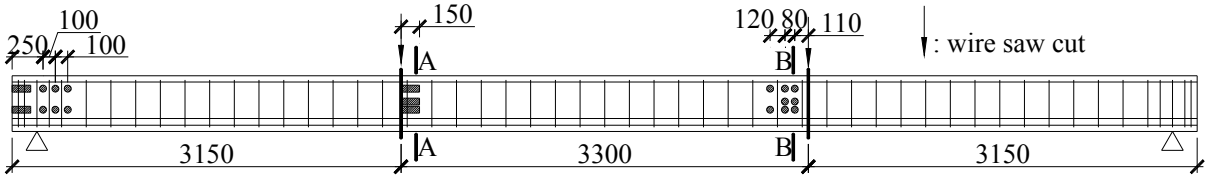

(a) Wire saw cutting positions

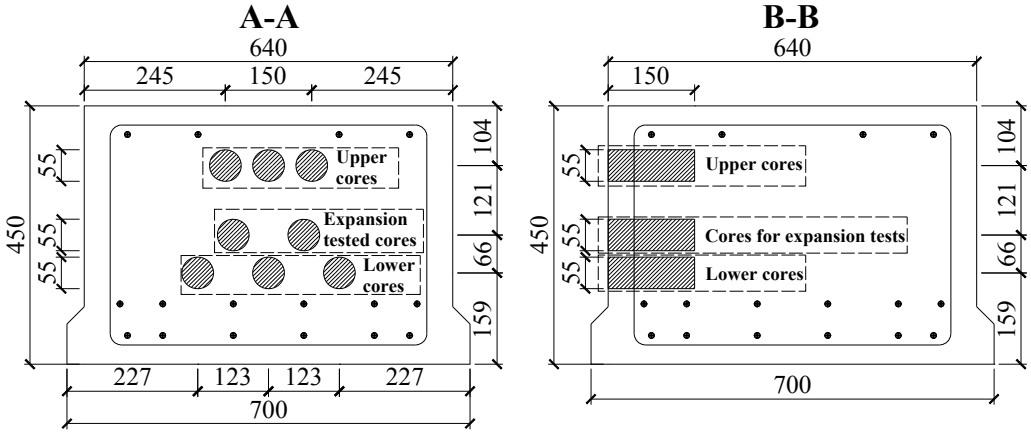

(b) longitudinal direction (c) transverse direction

Fig. 18(a)-(c) Test piece sampling locations. (unit: mm)

Table 5 Mechanical properties of core and ultrasonic wave propagation velocity.

Core collecting position			Compression strength (N/mm^2)		Modulus of elasticity (N/mm^2)		Ultrasonic wave propagation velocity (m/s)	
			H	FA	H	FA	H	FA
End part	longitudinal direction	Upper part	49.9	79.4	16.8	28.9	3870	4310
		Lower part	53.3	102.2	20.9	36.5	3990	4560
	transverse direction	Upper part	62.0	94.5	19.2	34.2	3970	4530
		Lower part	69.4	103.2	18.2	38.4	3880	4790
Central part	longitudinal direction	Upper part	68.0	102.0	24.2	41.1	4130	4770
		Lower part	75.7	89.5	27.8	42.9	4170	4800
	transverse direction	Upper part	43.4	109.1	14.5	36.8	3820	4620
		Lower part	58.5	111.4	18.9	39.3	3900	4780

the surface layer of concrete due to alkali outward flow and immobilization under alternation of drying and moistening processes (Kawamura 2010).

5.3 Expansion rate of concrete cores

The expansion rate of core obtained by the immersion method in 1N NaOH solution is indicated in **Fig. 21**. After one and a half years of outdoor exposure, because there were a large number of unreacted andesite particles, the cores of H girder expanded significantly up to 0.5% after being immersed in 1N NaOH solution maintained at 80 ºC. According to ASTM C1260 (2014), a specimen with an expansion rate of 0.2% or more after two weeks of soaking should be evaluated as "harmful". Therefore, both H and FA specimens were judged as "harmful" in this study. From **Fig. 21**, the expansion rate of H girder in the transverse direction was higher than in the longitudinal direction. This result is considered to be influenced by the difference in generation degree of fine cracks due to the collecting direction and the influence of restraint of PC tendons, that is to say, by the difference in the permeability of NaOH solution at the time of the test. The effects of the confinement degree due to prestressing on mechanical properties of concrete are discussed in the next section. Regarding a reference threshold value of hydroxide ion (OH^-) concentration in a pore solution for ASR initiation, Diamond (1983) proposed a value of 250 mmol/l (0.25 N), which was also confirmed and evaluated by other researchers (Rasheeduzzafar and Ehtesham Hussain 1991; Kagimoto *et al*. 2000, 2001; Kawabata *et al*. 2013). Therefore, it can be considered that unreacted other particles also reacted and thereby accelerated ASR when the concrete cores were soaking in 1N NaOH solution. This conclusion is useful in diagnosing ASR deterioration of core utilizing the immersion method in 1N NaOH solution at 80 ºC. Meanwhile, regarding FA girder, because of a slight generation of ASR, together with a low penetration of alkaline solutions, and an additional effect of alkaline adsorption of CSH with a low C/S ratio generated during pozzolan reaction, the measured expansion rate was remarkably lower than that of H girder.

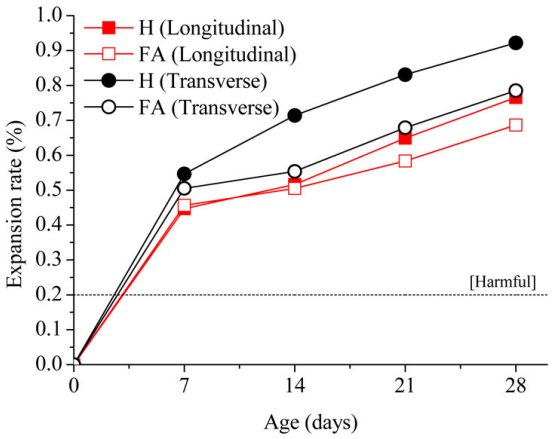

Fig. 21 Expansion rate of cores.

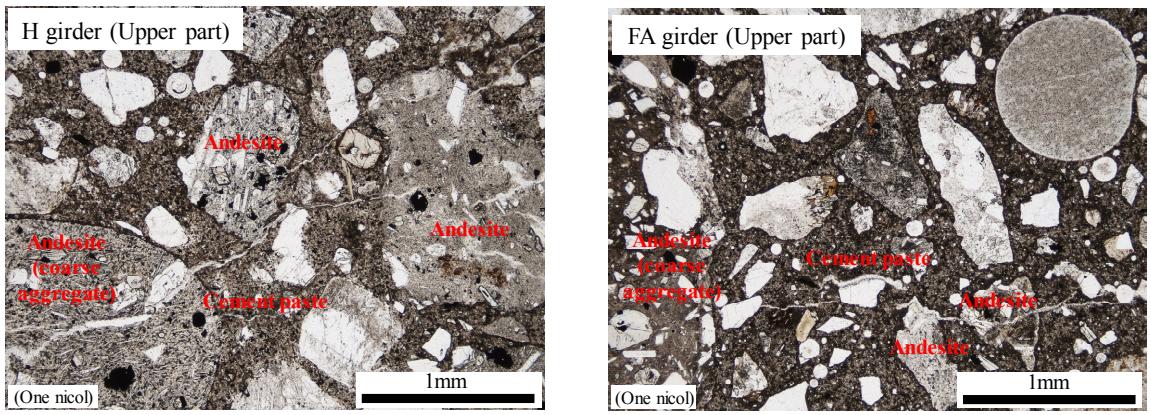

Fig. 20 Observation result of core slice by polarized microscope.

5.4 Mechanical properties of cores and ultrasonic wave propagation velocity

Table 5 indicates average values of compressive strength, static elastic modulus and ultrasonic wave velocity of concrete cores. Both the compressive strength and the elastic modulus of cores taken from H girder were smaller than from FA girder. Owing to the influence of fly ash content, the compressive strength and the elastic modulus of FA specimen were about 1.3 to 2 times greater than of H specimen. Compared to the compressive strength at 28 days (**Table 3**), the compressive strength of H specimen decreased significantly due to deteriorations caused by ASR. A previous study (Inagaki *et al*. 2009) pointed out that due to the influence of restraint of PC tendons, the compressive strength of concrete depended on direction when taking samples, this study also found out the same conclusion. Specifically, when comparing the test results of the upper part and the lower part of a cross section, the compressive strength and the static elastic modulus of cores taken from the lower part in the girder axis (near two lower layers of PC strands) were larger than those taken from the upper one. Moreover, as compared to results obtained from concrete samples of the central part, both the compressive strength and the elastic modulus of the end part were almost lower. The difference in both mechanical properties came up to approximately 30% on concrete cores collected in the longitudinal direction of H girder. In addition, because of the effect of restraining stress of PC strands together with the low expansion rate of concrete, the concrete samples collected longitudinally in the central part of H girder performed higher compressive strength in comparison with the samples taken in the transverse direction.

The relationship between compressive strength and static elastic modulus/compressive strength ratio of the concrete cores was shown in **Fig. 22**. In this figure, it was cleared that if the ASR damage in concrete become more severe, the measurement points will get closer to the origin from the curve showing healthy concrete **(**JSCE 2012**)**. In the case of FA girder, the obtained results were almost close to the healthy curve. Meanwhile, all points of H girder distributed away from the curve and toward the origin. It was considered that the influence of fine cracks owing to ASR and peeling of the aggregate interface was reflected by the decrease in compressive strength and static elastic modulus. **Figures 23 and 24** show the relationship between ultrasonic wave velocity with compressive strength and static elastic modulus of concrete cores, respectively. Because ultrasonic wave propagation can be easily measured on site, it is commonly used in structural health evaluation. As can be seen in **Figs. 23 to 24**, along with the ASR progression, the compressive strength and the static elastic modulus decrease linearly, and both parameters have a substantially proportional relationship to the ultrasonic wave velocity.

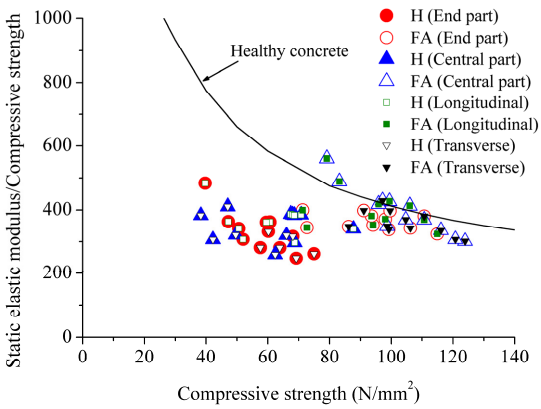

Fig. 22 Relationship between compressive strength and static elastic modulus/compressive strength ratio.

5.5 Recommendations on diagnosis of ASR degradation using concrete cores

From the test results, it is necessary to pay attention to two points when studying the relationship between the compressive strength, the static elastic modulus and the ultrasonic propagation velocity.

1) The first point is that the compressive strength of core taken from the transverse direction of central part of

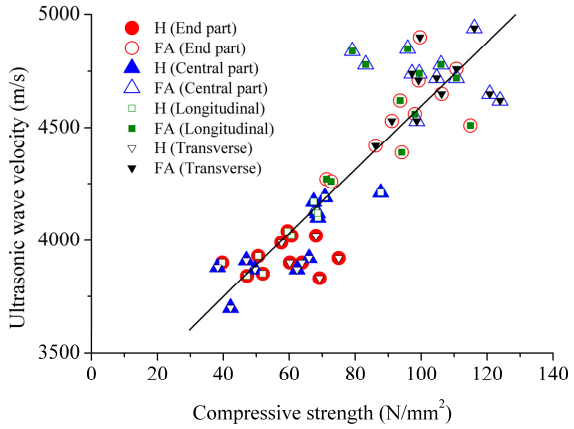

Fig. 23 Relationship between compressive strength of core and ultrasonic propagation velocity.

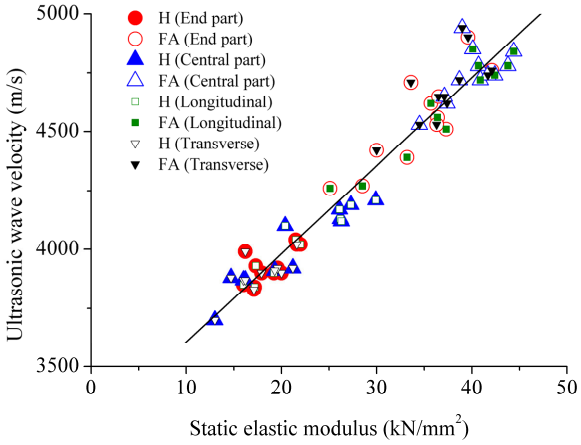

Fig. 24 Relationship between static elastic modulus of core and ultrasonic propagation velocity.

Fig. 25 Cracks occurred at the end of PC girder due to ASR-induced deformation.

ASR-affected girder reduced by about 30% as compared to the value measured from the longitudinal direction. Moreover, when comparing results obtained in the central and the end parts, except for some measurement results, the concrete cores of the end part have lower mechanical properties than of the central part. Especially, with respect to concrete cores collected in the longitudinal direction of H girder, the difference in both mechanical properties came up to approximately 30%.

2) The second point is that the compressive strength and the static elastic modulus of concrete cores might decrease due to the effects of water and stress release during the coring. Therefore, when calculating load-carrying capacity and reinforcement design for ASR-degraded PC girders, it is necessary to perform an appropriate correction according to the constraint degree owing to the prestress instead of using the measurement values of the cores directly.

Furthermore, as can be seen in **Fig. 25**, the difference in expansion rate between the upper and the lower sides of a girder induced a large deformation (upward warpage), and it might lead to new damage. Therefore, it is desirable to check the damage caused by local destruction at the girder end and by dismounting of PC anchoring parts simultaneously at the time of inspection for PC bridges. Regarding long-term prospects, further research should be carried out on the subject.

6. Conclusions

In this study, two PC girders, which were constructed and placed outside the laboratory, had been exposed to weather conditions for one and a half years. The first girder was affected by alkali-silica reaction while the second one was kept at an inactive state with ASR acceleration due to the addition of fly ash. Then, using the destructive loading test, this study investigated the difference in load carrying capacity of two PC girders due to the presence or absence of fly ash. Moreover, after the destructive loading test, the effects of the sampling position and direction of the concrete core on changes in compressive strength, static elastic modulus, and ultrasonic wave propagation velocity were analyzed and discussed by collecting concrete cores from both PC girders affected by ASR deterioration. The main results obtained from this study are summarized as follows.

1) After one and a half year of monitoring of cracks, an addition of fly ash played a significant role in mitigating the cracks caused by the expansion due to ASR.
2) An increase of convex curvature was observed in the girder without fly ash. After monitoring period, the convex displacement increased up to ~13 mm before starting the load test with respect to H girder. Meanwhile, almost no change in convex curvature over time was observed in FA specimen mixed with fly ash.
3) An addition amount of fly ash did not only increase the load bearing capacity by nearly 5% but also enhance the initial bending stiffness of the objective PC girder by 10% after more than one year under ASR deteriorations.
4) From observation results of cut cross-section after the loading test, the depth of ASR-induced cracks along the girder-axis direction varied from 5 to 20 mm on the side surfaces and the top surface. However, no crack was found out in the area surrounded by stirrups, and no breaking of tendons was confirmed.
5) Regarding H specimen, andesite particles from sand and gravel reacted strongly, and many fine cracks (about 0.02 mm in width) occurred from broken pieces of aggregates to cement paste. However, because of the slight reaction of andesite particles, no trace of ASR was observed on FA specimen.
6) When the concrete cores of H girder were soaking in 1N NaOH solution, unreacted andesite particles accelerated ASR leading to high expansion rate. Meanwhile, regarding FA girder, the expansion rate was significantly low as compared to that of H girder.
7) Proportional correlations between the compressive strength, the static elastic modulus and the ultrasonic propagation velocity of the core were found.
8) Results of the coring test shown that the mechanical properties of concrete cores varied according to their collecting positions and directions. Therefore, when assessing the load-carrying capacity and mechanical properties of PC girder under ASR deterioration, it is necessary to make appropriate corrections according to the confinement degree due to prestressing instead of using measured values of the concrete core as they are.

Acknowledgement

This research was promoted by the Cross-Ministerial Strategic Innovation Promotion Program [Title: Resolution of Early-aged Deterioration Mechanisms in Concrete Bridges and Development of Total Management

System Based on Evaluation for Material and Structure Quality Performance, Kanazawa University] from the Japan Science and Technology Agency (JST). The authors wish to thank the concerned parties for their valuable collaboration, sub-consultants, and support.

References

ASTM International, (2014). "*ASTM C1260-14: Standard test method for potential alkali reactivity of aggregates* (*Mortar-bar method*)." West Conshohocken, PA.

Diamon, S., (1983). "Alkali reactions in concrete- Pore solution effects." *Proceedings of 6th International Conference on Alkali-Aggregate Reaction in Concrete*, Copenhagen 1983, 155-166.

Fournier, B. and Bérubé, M. A., (1991a). "Application of the NBRI accelerated mortar bar test to siliceous carbonate aggregates produced in the St. Lawrence Lowlands (Quebec, Canada) Part 1: Influence of various parameters on the test results." *Cement and Concrete research*, 21, 853-862.

Fournier, B. and Bérubé, M.A., (1991b). "Application of the NBRI accelerated mortar bar test to siliceous carbonate aggregates produced in the St. Lawrence Lowlands (Quebec, Canada) Part 2: Proposed limits, rates of expansion, and microstructure of reaction products." *Cement and Concrete research*, 21, 1069-1082.

Gasparotto, G., Bargossi, G. M., Peddis, F. and Sammassimo, V., (2011). "A case study of alkali-silica reactions: petrographic investigation of paving deterioration." *Periodico di Mineralogia*, 80(2), 309-316.

Giaccio, G., Zerbino, R., Ponce, J. M. and Batic, O. R, (2008). "Mechanical behavior of concretes damaged by alkali-silica reaction." *Cement and Concrete Research*, 38, 993-1004.

Gong, F., Takahashi, Y. and Maekawa, K., (2017). "Strong coupling of freeze-thaw cycles and alkali silica reaction - multi-scale poro-mechanical approach to concrete damages -." *Journal of Advanced Concrete Technology*, 15, 346-367.

Hajighasemali, S., Ramezanianpour, A. and Kashefizadeh, M., (2014). "The effect of alkali-silica reaction on strength and ductility analyses of RC beams." *Magazine of concrete research*, 66(15), 751-760.

Hashimoto, T. and Torii, K., (2013). "The development of highly durable Concrete using classified fine fly ash in Hokuriku district." *Journal of Advanced Concrete Technology*, 11, 312-321.

Hashimoto, T. and Torii, K., (2015). "The assessment on ASR of aggregates and ASR mitigation effect by fine fly ash." *Concrete in Australia*, 42(2), 65-71.

Hiroi, Y., Yamamoto, T., Toda, Y., Manabe, H. and Miyagawa, T., (2016). "Experimental and analytical studies on flexural behaviour of post-tensioned concrete beam specimen deteriorated by alkali-silica reaction (ASR)." In: H. M. Bernardes and N. P. Hasparyk, Eds. *15th International Conference on Alkali-Aggregate Reaction*, Sao Paulo Brazil 03-07 July 2016.

Hirono, S., Ando, Y., Satoh, T., Yamada, K., Kagimoto, H. and Torii, K., (2016). "ASR found in Thailand and tropical regions of Southeast Asia." In: H. M. Bernardes and N. P. Hasparyk, Eds. *15th International Conference on Alkali-Aggregate Reaction*, Sao Paulo Brazil 03-07 July 2016.

Hong, S. H., Han, S. H. and Yun, K. K., (2007). "A case study of concrete pavement deterioration by alkali-silica reaction in Korea." *International Journal of Concrete Structures and Materials,* 1(1), 75-81.

Inagaki, T., Obana, Y., Ishii, T. and Torii, K., (2009). "Mechanical properties of core collected from ASR degraded PC beam specimen." *Proceedings of the Japan Concrete Institute*, 31(1), 1237-1242. (in Japanese)

Japan Meteorological Agency, (2016). http://www.jma.go.jp/jma/index.html. Accessed April 2015-October 2016

Japan Society of Civil Engineers Concrete Committee, (2012). "*Standard specifications for concrete structures: Design*." (in Japanese; 2007, now in English)

Kagimoto, H., Sato, M. and Kawamura, M., (2000). "Evaluation of the degree of deterioration in ASR damaged concretes and analyses of their pore solutions." *Journal of Japan Society of Civil Engineers*, 46(641), 241-251. (in Japanese)

Kagimoto, H., Sato, M. and Kawamura, M., (2001). "OH^- ion concentration limit of pore solution of mortar using several different reactive aggregates." *Proceedings of the Japan Concrete Institute,* 23(2), 589-594. (in Japanese)

Katayama, T., Tagami, M., Sarai, Y., Izumi, S. and Hira, T., (2004). "Alkali-aggregate reaction under the influence of deicing salts in the Hokuriku district, Japan." *Materials Characterization*, 53, 105-122.

Kawabata, Y., Yamada, K. and Matsushita, H., (2013). "Relation of phase composition of cement hydrates with supplementary cementitious materials to the suppressing effect on ASR expansion." *Journal of Japan Society of Civil Engineers, Ser. E2* (*Materials and Concrete Structures*), 69(4), 402-420. (in Japansese)

Kawamura, M., (2010). "*Alkali-silica reaction in concrete*." Seiunsha, 36-54. (in Japansese)

Kobayashi, K., Inoue, S., Yamasaki, T. and Nakano, K., (1988). "Alkali aggregate reaction in prestressed concrete beams." *The international Journal of Cement Composites and Lightweight Concrete* 10(4), 233-240.

Kubo. T., Shibata, T., Sannoh, C. and Torii, K., (2016). "The reinforcement of an ASR affected intake tower using post-tensioneds." In: H. M. Bernardes and N.P. Hasparyk, Eds. *15th International Conference on Alkali-Aggregate Reaction*, Sao Paulo Brazil 03-07

July 2016.

Kunitomi, Y., Ishii, A., Xin, J. and Torii, K., (2015). "Characteristic of load-bearing capacity of PC beams using ground granulated blast furnace slag by ASR accelerated exposure test." *Journal of prestressed concrete*, 57(3), 68-74. (in Japanese)

Leemann, A., Thalmann, C. and Studer, W., (2005). "Alkali-aggregate reaction in Swiss tunnels." *Materials and Structures*, 38, 381-386.

Marfil, S. A. and Maiza, P. J., (2001). "Deteriorated pavements due to the alkali-silica reaction a petrographic study of three cases in Argentina." *Cement and Concrete Research*, 31, 1017-1021.

Miyagawa, T., Seto, K., Sasaki, K., Mikata, Y., Kuzume, K. and Minami, T., (2006). "Fracture of reinforcing steels in concrete structures damaged by alkali-silica reaction- Field survey, mechanism and maintenance-." *Journal of Advanced Concrete Technology*, 4(3), 339-355.

Oberholster, R. E. and Davies, G., (1986). "An accelerated method for testing the potential alkali reactivity of siliceous aggregates." *Cement and Concrete research*, 16, 181-189.

Ono, K., (1988). "Damaged concrete structures in Japan due to alkali silica reaction." *The International Journal of Cement Composites and Lightweight Concrete*, 10(4), 247-257.

Onozato, M., Kobayashi, T., Ogawa, S. and Matsubayashi, Y., (2006). "Flexural bearing capacity of prestressed concrete damaged by ASR." *Proceedings of the Symposium on Developments in Prestressed Concrete*, 15, 97-100. (in Japanese)

Rasheeduzzafar and Ehtesham Hussain, S., (1991). "Effect of microsilica and blast furnace slag on pore solution composition and alkali-silica reaction." *Cement & concrete composites*, 13, 219-225.

Sannoh, C., Maruyama, T., Yamato, H. and Torii, K., (2013). "Development of simple ASR diagnostic technique by gel fluorescence method." *Proceedings of the Japan Concrete Institute*, 35(1), 973-978. (in Japanese)

Stanton, T. E., (1940). "Expansion of concrete through reaction between cement and aggregate." *Proceedings of the American Society of Civil Engineers*, 66, 1781-1811.

Saouma, V. E., (2014). "*Numerical modeling of AAR*." Taylor & Francis.

Shehata, M. H. and Thomas, M. D. A., (2000). "The effect of fly ash composition on the expansion of concrete due to alkali-silica reaction." *Cement and concrete research*, 30, 1063-1072.

Shenfu, F. and Hanson, J. M., (1998). "Effect of alkali silica reaction expansion and cracking on structural behavior of reinforced concrete beams." *ACI Structural Journal*, 95(5), 498-505.

Swamy, R. N. and Al-Asali, M. M., (1989). "Effect of alkali-silica reaction on the structural behavior of reinforced concrete beams." *ACI Structural Journal*, 86(4), 451-459.

Takahashi, Y., Ogawa, S., Tanaka, Y. and Maekawa, K., (2016). "Scale-dependent ASR expansion of concrete and its prediction coupled with silica gel generation and migration." *Journal of Advanced Concrete Technology*, 14(8), 444-463.

Takebe, Y., Tokoyama, T., Yonekawa, H., Nakamura, K. and Miyagawa, T., (2013). "Strengthening effect on prestressed concrete members affected by alkali-silica reaction (ASR)." In: P. Claisse, E. Ganjian and T. Naik, Eds. *Third International Conference on Sustainable Construction Materials and Technologies*, Kyoto Research Park Kyoto, Japan 18-21 August 2013.

Tomiyama, J., Yamada, K., Kaneda, K., Iraha, S. and Oshiro, T., (2011). "ASR diagnosis by petrographic investigation and evaluation of mechanical performance of ASR deteriorated pretensioned PC beam." *Journal of Japan Society of Civil Engineers, Ser. E2* (*Materials and Concrete Structures*), 67(4), 578-595. (in Japanese)

Tordoff, M. A., (1990). "Assessment of pre-stressed concrete bridges suffering from alkali-silica reaction." *Cement & Concrete Composites*, 12, 203-210.

Torii, K., (2010). "The characteristic feature of fracture of steel reinforcement in ASR-deteriorated concrete structures." *International Journal of Corrosion Engineering*, 59(4), 59-65.

Torii, K., Kubo, T., Sannoh, C. and Kanitani, M., (2016a). "The strengthening of an ASR-affected water intake tower in a hydro-electric dam by using post-tensioned tendons and the long-term monitoring of tower." *Journal of Advanced Concrete Technology*, 14, 384-396.

Torii, K., Kubo, T., Sannoh, C. and Kanitani, M., (2016b). "The alkali-silica reactivity of andesitic river aggregates and ASR mitigating effect by using fine fly ashes." In: H. M. Bernardes and N. P. Hasparyk, Eds. *15th International Conference on Alkali-Aggregate Reaction*, Sao Paulo Brazil 03-07 July 2016.

Torii, K., Okuyama, K., Kuzume, K. and Sasatanai, T., (2007). "Monitoring and strengthening methods of bridge pier seriously damaged by alkali-silica reaction." *Fifth International Conference on Concrete under Severe Conditions Environment and Loading*, Tours France 4-6 June 2007, 1, 787-794.

Torii, K., Prasetia, I., Minato, T. and Ishii K., (2012). "The feature of cracking in prestressed concrete bridge girders deteriorated by alkali-silica reaction." In: T. Drimalas, J. H. Ideker and B. Fournier, Eds. *14th International Conference on Alkali-Aggregate Reaction*, Austin Texas USA 20-25 May 2012.

Wang, J. and Morikawa, H., (2012). "Study on shear behavior of deteriorated RC beams due to alkali-silica reaction." *37th Conference on our world in concrete & structures*, Singapore 29-31 August 2012. CI-Premier Pte Ltd, 10 pages.

Yamada, K., Hirono, S. and Miyagawa, T., (2011). "New finding of ASR degradation in Japan." In: A. Palomo,

A. Zaragoza and J. C. L. Agüí, Eds. *13th International congress on the chemistry of cement,* Madrid 3–8 July 2011. CR-R, 7 p.

Yamamura, S., Sakurada, M., Kobayashi, K. and Torii, K., (2016). "Application of fly ash concrete to prestressed concrete bridges." *Cement & concrete*, 828, 22-27. (in Japanese)

Yokoyama, T., Miyagawa, T., Hiroi, Y., Yamamoto, T., Manabe, H. and Ookubo, T., (2016). "Long-term deterioration of quasi-actual scale prestressed concrete beam due to alkali-silica reaction." In: H. M. Bernardes and N. P. Hasparyk, Eds. *15th International Conference on Alkali-Aggregate Reaction*, Sao Paulo Brazil 03-07 July 2016.